The effects of anthropogenic greenhouse gases and aerosols on the inter-decadal change of the South China Sea summer monsoon in the late twentieth century

Article

Accepted Version

www.reading.ac.uk/centaur

CentAUR

Central Archive at the University of Reading

Reading's research outputs online

1 **The effects of anthropogenic greenhouse gases and aerosols on the inter-decadal change**

2 **of the South China Sea summer monsoon in the late 20th Century**

3 **Zhongxi Lin[1] Buwen Dong[2] Zhiping Wen[3]**

4 1 Center for Monsoon and Environment Research/School of Atmospheric Sciences, Sun Yat-sen
5 University, Guangzhou, China
6 2 Department of Meteorology, National Centre for Atmospheric Science, University of Reading,
7 Reading, UK
8 3 Department of Atmospheric and Oceanic Sciences & Institute of Atmospheric Sciences, Fudan

9 University, Shanghai, China

10

11

12

13

14

15

16

17

18

19 Corresponding author:

20 Zhongxi Lin,

21 Center for Monsoon and Environment Research/ School of Atmospheric Sciences

22 Sun Yat-Sen University,

23 Zhuhai, 519082 China

24 E-mail: linzhxi@mail2.sysu.edu.cn

26 **Abstract:** Analysis of observational precipitation indicates that in last few decades, the

27 precipitation in boreal summer (June-August) over the South China Sea (SCS) exhibited an

28 interdecadal variation, characterized by a decrease of 0.59mm/day from the period 1964-

29 1981 to the period 1994-2011. Accompanied this decrease in precipitation is weakened

30 monsoon circulation featured by an anti-cyclonic circulation anomaly over the SCS in the

31 later period relative to the early period. This work investigates impacts of anthropogenic

32 forcing changes on this interdecadal change in observations, quantify the relative roles of

33 greenhouse gases (GHG) forcing and anthropogenic aerosol (AA) forcing. A set of

34 experiments is designed using the atmospheric component of a state-of-the-art climate

35 model coupled to a multi-level mixed-layer ocean model forced with GHG concentrations

36 and AA emissions in two periods.   Modeling results indicate a dominant role of

37 anthropogenic forcing on the observed interdecadal precipitation decrease and weakened

38 monsoon circulation over the SCS in the late 20th century in which AA forcing plays a more

39 important role compared with GHG forcing. The mechanisms of GHG influences and AA

40 induced changes are revealed by individual forcing experiments. Increasing GHG

41 concentrations can suppress convection over the SCS summer monsoon (SCSSM) region

42 by warming the tropical Pacific with an El-Niño like sea surface temperature (SST) pattern,

43 which is associated with a weakened Walker circulation. The changes in AA emissions,

44 mainly through increases in emissions over Asia, lead to cool SST in the north Indian Ocean

45 and the western North Pacific (WNP), and result in changes in meridional SST gradient over

46 the tropical Indian Ocean and the WNP in pre-monsoon seasons. This anomalous

47 meridional SST gradient leads to anomalous local Hadley circulation, characterized by

48 anomalous ascents around the equator and descents over monsoon region, which

49   suppresses convection over the SCS and reduces local precipitation.

50   **Key words**: South China Sea summer monsoon, anthropogenic greenhouse gases,

51   anthropogenic aerosols, precipitation.

52

53   **1 Introduction**

54   The South China Sea (SCS) locates in Southeast Asia between the equator and South

55   China coast, from 110°E to 120°E. It is in the center of the Asian-Australian monsoon system

56   and has a close relation with the East Asian monsoon, South Asian monsoon and Western

57   North Pacific monsoon due to geographic location (Tao and Chen 1987; Ding 1992,

58   Murakami and Matsumoto 1994; Wang 1994; Lau and Yang 1997). The climate over the

59   SCS is mainly controlled by monsoon circulation, characterized by a warm and wet westerly

60   low-level flow during boreal summer, and cold and dry easterly low-level flow during winter.

61   In summer, westerly flow comes from the Indian Ocean, turns into southerly and transports

62   moisture to the East Asian monsoon region. Over the SCS, this cyclonic circulation forms a

63   local monsoon trough and leads to convection and abundant precipitation.

64   The SCS summer monsoon (SCSSM) changes in multiple time-scales (Zhou et al. 2005;

65   Wang et al. 2009; Tong et al. 2009) and can be affected by many different factors, including

66   solar radiation on orbital time scale (Prell 2011), interdecadal time scale, and sea surface

67   temperature (SST) variability and land-sea thermal contrast on interannual time scale (Wang

68   and Zhang 2002; Lau et al. 2004; Zhou et al. 2005; Lau and Wang 2006; Yuan et al. 2008;

69   Wang and Qian 2009; Zhu et al. 2011). Its intensity is sensitive to the definition since the

70   SCSSM can be affected by the multiple monsoon subsystems, including the East Asian

71   summer monsoon (EASM), South Asian summer monsoon (SASM), and western North

72   Pacific summer monsoon (WNPSM). Previous researches use some indices to describe

73   characteristics of the SCSSM, including its southwesterly low-level flow, local convection

74   and moisture transport convergence (Lu and Chan 1999; Liang et al. 1999; Li and Zhang

75   1999; Dai et al. 2000; Liang et al. 1999; Wu and Liang 2001; Yao and Qian 2001; Zhang et

76   al. 2002; Wen et al. 2006; Wang et al. 2008). A meridional shear vorticity index (zonal wind

77   in the south SCS minus that in the north SCS; Wang et al. 2009) is created to describe the

78   strength of the SCSSM and is then widely used. Based on 7-year mean of this index, inter-

79   decadal changes are observed in the early 1970s and the early 1990s (Wang et al. 2009).

80   However, drivers and physical mechanisms for these interdecadal changes are not fully

81   investigated.

82   The interdecadal variation of the EASM and SASM has been attributed to both internal

83   variability associated with low frequency SST variability in the Atlantic and Pacific (i.e., the

84   Pacific Decadal Oscillation [PDO] and the Atlantic Multidecadal Oscillation [AMO], Goswami

85   et al. 2006; Lu et al. 2006; Zhou et al. 2009) and external forcing associated with changes

86   in greenhouse gases (GHG) and anthropogenic aerosol (AA) emissions (Song et al. 2014;

87   Li et al. 2015; Li and Ting 2017, Tian et al. 2018, Luo et al. 2019). Most of previous studies

88   agree that precipitation tends to increase in both EASM and SASM due to increased

89   moisture content in the atmosphere with increasing GHG forcings. Despite of the increased

90   moisture content, the effect of GHG and AA on the monsoon circulation is important and

91   requires further research.

92   The greenhouse gases (GHG) can change the SASM monsoon circulation by changing

93   the large-scale tropical Walker circulations and land-sea thermal contrast (Ueda et al. 2005).

94   In some model studies, the intensity of the Walker circulation connecting the tropical Pacific

95 and monsoon region tends to be weakened (Tanaka et al. 2004; Ueda et al. 2005, May 2002,

96 Vecchi and Soden 2006; Lau and Kim 2017), which suppresses the convection in the SASM

97 region. The land-sea thermal contrast is increased as the temperature over land response

98 to GHG increases is stronger than over ocean (Sutton et al. 2007; Dong et al. 2009). The

99 land-sea thermal contrast between South Asia and Indian ocean, which is an important

100 driver of the SASM (Wu et al. 2012), could lead to an enhanced circulation (Hu et al. 2000).

101 However, the weakened thermal contrast in the upper troposphere might play a more

102 important role in a long-term trend and weakened SASM monsoon circulation (Sun et al.

103 2010). For the EASM, Jiang and Wang (2005) and Song et al. (2014) suggested that the

104 summer monsoon circulation over East Asia is slightly enhanced based on model

105 ensembles. It is further revealed that the increased GHG leads to enhanced western North

106 Pacific Subtropical High (WNPSH) and increased southerly on the western boundary of

107 WNPSH (Tian et al. 2018). Over ocean, Lee et al. (2008) suggested that the low-level

108 convergence decreases over the western North Pacific and the WNPSM weakens despite

109 of increasing moisture in the atmosphere in response to CO_2 increases.

110   Some anthropogenic aerosols (AA) can cause surface cooling by scattering and

111 absorbing solar radiation and change the radiative properties of clouds (Boucher et al. 2013).

112 Meanwhile, black carbon and organic carbon can absorb reflected solar radiation to increase

113 the atmospheric temperature (Menon et al. 2002; Ming et al. 2010; Ramanathan et al. 2001).

114 As AA emissions increased during the last few decades in Asia, it might affect the adjacent

115 precipitation by altering the land-sea thermal contrast and relative monsoon circulation (Ming

116 and Ramaswamy 2011; Rotstayn and Lohmann 2002; Dong et al. 2016). In SASM region,

117 the monsoon circulation changes in response to increased AA emissions are characterized

118   by an anomalous meridional overturning circulation that tends to decrease precipitation over

119   the Indian peninsula (Bollasina et al. 2011). Some model studies suggest the resulted

120   anomalous meridional SST gradient over the Indian Ocean with cooling on the North Indian

121   Ocean in response to AA emission changes is the main driver (Ganguly et al. 2012; Ganguly

122   et al. 2012; Ramanathan et al. 2005; Chung et al. 2006; Luo et al. 2019). In EASM region,

123   observations show a wet trend in south China and a drought trend in north in past several

124   decades and this pattern is considered as a result of increased aerosol emissions in China

125   (Wang 2001; Ding et al. 2008, 2009; Menon et al. 2002; Xie et al. 2016; Tian et al. 2018).

126   Some studies suggest that the aerosol can cause a regional cooling over land and leads to

127   a weakened land-sea thermal contrast and thus weakened EASM circulation and

128   precipitation (Ye et al. 2013; Song et al. 2014, Dong et al. 2016).

129   In Asian monsoon region, GHG and AA do not always play similar roles for the monsoon

130   decadal variations. Lau and Kim (2017) suggested that increases in GHG since 1950s

131   generate an increased land-sea thermal contrast but it is masked by the cooling induced by

132   AA forcing. This study also suggested that the EASM and SASM are having different

133   sensitivity to GHG and AA changes. In EASM region, as the circulation is weakened by AA

134   effect while GHG's role is negligible due to the offset by its dynamic effect and

135   thermodynamic effect, AA forcing is more dominating in the decreased monsoon circulation

136   and tends to reduce the precipitation (Zhang and Li 2016; Song et al. 2014). Luo et al. (2019)

137   suggested that reduction in precipitation in South Asia in last few decades is related to the

138   weakened SASM circulation in response to changes in both GHG and AA and that

139   circulation change induced precipitation decrease is stronger than the increase related to

140   moisture increase in the atmosphere. All above mentioned studies are on changes of GHG

141 and AA emissions on either the EASM or SASM. In contrast, the anthropogenic influences

142 on the SCSSM and physical processes involved are not fully investigated.

143   This study aims to elucidate the processes of how GHG and AA affect the inter-decadal

144 change of the SCSSM in the late 20th century, focusing on: 1) What is the role of

145 anthropogenic forcing to the observed inter-decadal change? 2) What are the relative roles

146 of changes in GHG and AA frocings? 3) What are the physical processes? We have

147 performed a set of model experiments using the atmospheric component of the state-of-the-

148 art HadGEM3 global climate model coupled to a multi-level mixed-layer ocean model to

149 address these questions.

150   Lots of studies about impacts of anthropogenic forcings on the EASM and SASM use

151 full ocean Coupled General Circulation Models (CGCM) including CMIP5 models (Song et

152 al. 2014; Seo et al. 2013; Chen et al. 2016; Sharmila et al. 2015), but these models usually

153 have significant bias on sea surface temperature (SST) in mean state (Li et al. 2012; 2015;

154 Levine et al. 2013). As the Australian-Asian monsoon is sensitive to SST, this bias may

155 cause even larger bias on monsoon simulation. Thus, MetUM-GOML models use an ocean

156 mixed-layer model replacing the 3D CGCMs, which can reduce the calculation cost and

157 have a smaller SST bias by a prescribed flux corrections (Hirons et al. 2015, Dong et al.

158 2017, Tian et al. 2018). So, this work will use a set of experiments based on the second

159 generation of GOML models (MetUM-GOML2).

160   The structure of this paper is as follows: Section 2 analyses the observational data and

161 describes the inter-decadal change of the SCSSM in the late 20th century. Section 3

162 introduces the model and detailed design of model experiments. Section 4 evaluates the

163 relative contributions of different forcings to the inter-decadal change. Sections 5 and 6

164 reveal the physical processes of changing GHG or AA forcing on the SCSSM respectively.

165 Finally, our conclusions are drawn in Section 7.

166

167 **2 Observed inter-decadal change**

168 In this study, we use monthly NOAA's Precipitation Reconstruction (PREC) dataset

169 (Chen et al. 2002) and precipitation based on GPCP (Adler et al. 2003). Observed 3D

170 monthly horizontal velocity and vertical velocity come from NCEP Reanalysis 1 (NCEP1;

171 Kalnay et al. 1996) while monthly sea level pressure (SLP) is obtained from Hadley Centre

172 Sea Level Pressure dataset (HadSLP2; Allan and Ansell 2006). All variables are averaged

173 from June to August to describe the boreal summer mean.

174 To show the inter-decadal variability (IDV) of rainfall change in observations, the area

175 averaged precipitation in the South China Sea region (10°N-20°N, 105°E-120°E) in JJA is

176 defined as an index and its time evolution is shown in Figure 1a. One of the most important

177 features of the time evolution of this precipitation index is the inter-decadal variation across

178 the 1990s, characterized by a positive precipitation anomaly from 1964 to 1981 (early period,

179 EP) and a negative precipitation anomaly from 1994 to 2011 (present day, PD). These

180 periods are selected also to avoid the impact of volcanic eruptions. The mean anomaly in

181 these two periods is 0.45 mm/day in EP and -0.14 mm/day in PD, respectively, which means

182 a -0.59 mm/day (which is about 13.6% of the climatological mean of 1979-2018 in GPCP

183 dataset) decrease from EP to PD.

184 We compare the spatial pattern of precipitation and circulation associated with this inter-

185 decadal change (PD minus EP) to understand the physical processes involved. It is found

186 that the inter-decadal decrease in precipitation mainly centered in the SCS (up to 0.5-2.0

187   mm/day), and was accompanied by anomalous anticyclonic circulation in the lower

188   troposphere (fig. 1b) with anomalous easterlies across the SCS. The anomalous easterlies

189   over the SCS indicate weakened climatological SCS westerlies in the summer from EP to

190   PD. The anomalous anticyclonic circulation is also associated with anomalous divergence

191   in the lower troposphere and anomalous convergence in the upper troposphere (Fig. 1c)

192   with anomalous descent in the whole troposphere (Fig. 1d), indicating weakened convection

193   in the SCS and therefore leading to reduced precipitation.

194   What had caused this inter-decadal decrease in precipitation and monsoon circulation

195   over the SCS seen in observations? To find out drivers and understand the dynamical

196   mechanisms behind it, we perform a set of time slice experiments with the atmospheric

197   component of the state-of-the-art HadGEM3 global climate model coupled to a multi-level

198   mixed-layer ocean model with changes in GHG and AA emissions together from EP to PD

199   or changes in GHG and AA forcing separately.

200

201   **3 Models and experiments**

202   **3.1 MetUM-GOML2 model and experiments settings**

203   In this work, MetUM-GOML2 (e.g., Hirons et al. 2015) is used to perform a set of

204   experiments. The atmospheric component of the MetUM-GOML2 is the Met Office Unified

205   Model (MetUM) at the fixed scientific configuration Global Atmosphere 6.0 (GA6.0) with N96

206   horizontal resolution (1.875° longitude and 1.25° latitude) and 85 vertical levels. A detailed

207   description of GA6.0 is given by Walters et al. (2017). The atmospheric model includes an

208   interactive tropospheric chemistry scheme (eight aerosol species are included: ammonium

209   sulphate, mineral dust, fossil fuel black carbon, fossil-fuel organic carbon, biomass-burning,

210 ammonium nitrate, sea-salt, and secondary organic aerosols from biogenic emissions. Both

211 aerosol-radiation interaction and aerosol-cloud interaction (including aerosol indirect effect

212 and semi-indirect effect) are considered. More details about the parameterization of aerosol

213 indirect effect are described by Jones et al. (2011) and Bellouin et al. (2011, 2013).

214   The oceanic component is a Multi-Column K Profile Parameterization mixed-layer ocean

215 model. The horizontal resolution of MC-KPP is the same as AGCM where they are coupled,

216 and below each AGCM grid point in ocean region is one water column. The atmospheric

217 and oceanic components are coupled every 3 hours. Since MC-KPP only simulate vertical

218 mixing in each grid point and exclude the ocean dynamics, the climatological seasonal

219 ocean 3D flux corrections are applied on ocean temperature and salinity (Large et al. 1994).

220 These corrections are intended to represent the mean advection in ocean and account for

221 biases in atmospheric surface fluxes.

222   The set of experiments used in this study is the same as those used to investigate SASM

223 decadal changes in Luo et al. (2019). Here, we use greenhouse gases (GHG) and

224 anthropogenic aerosol (AA) forcings averaged over 1994-2011 as PD conditions. For EP

225 forcing, GHG forcing is an average of 1964-1981 while AA forcing is an average of 1970-

226 1981. The details of experiments are summarized in Table 1. Firstly, a relaxation experiment

227 is run for 12 years (E0) forced by PD GHG and AA forcing. In this experiment, the MC-KPP

228 profiles of temperature and salinity were relaxed to a PD climatological ocean temperature

229 and salinity from the Met Office ocean analysis data (Smith and Murphy 2007). Then we

230 diagnosed the seasonal cycle of climatological daily-mean 3D ocean temperature and

231 salinity corrections from E0. These temperature and salinity are the same and are imposed

232 in all free running coupled experiments. Therefore, response in the model experiments to a

233 particular forcing change includes both the fast response to the forcing change (i.e. surface

234 and atmospheric process) and slow response mediated by forcing induced SST change.

235 For free coupled experiments, the EP experiment (EP) is forced by GHG and AA forcing of

236 EP while All forcing present day (PD-ALL) is forced by PD GHG and AA forcing. In addition,

237 two extra experiments, present-day GHG forcing (PD-GHG) with PD GHG but EP AA and

238 present-day AA forcing (PD-AA) with PD AA but EP GHG, that are used to analyze the

239 individual effect of GHG and AA. All coupled experiments are run for 60 years and only last

240 55 years of each experiment are used for analysis. In all experiments, the annual mean

241 concentrations of GHG are prescribed uniformly globally while the aerosol emissions include

242 seasonal cycle and spatial distribution. The spatial distribution of changes in annual mean

243 sulphur dioxide emissions between the two periods was illustrated in the Fig. 3 in Chen and

244 Dong (2019) where changes are characterized by decreases over North America and

245 Europe and increases over South Asia and East Asia.

246 The response of different forcing is estimated by the difference of climatology between

247 a pair of experiments. The difference of PD-ALL and EP represent the combine effect of

248 GHG and AA forcing difference, while PD-GHG minus EP and PD-AA minus EP are

249 estimation of individual effect of GHG forcing and AA forcing. The statistical significance of

250 the difference in a pair of models is assessed using a two tailed Student's t-test.

251

252 **3.2 Model climatology**

253 In this section, some climatological features of PD experiment are compared with

254 observations. Fig.2a and b show the precipitation, SLP and 850hPa wind from June to

255 August (JJA) in PD-ALL forcing experiment and Fig.2c and d show the SLP and 850hPa

256 wind from NCEP reanalysis 1 and observed precipitation from Global Precipitation

257 Climatology Project (GPCP; Adler et al. 2003). In observations, spatial pattern of SLP is

258 characterized by low SLP over the Eurasia continent and high SLP on the tropical Indian

259 ocean and western North Pacific (WNP). This SLP distribution is associated with westerly

260 monsoon flow from India and it turns into southwesterly with cyclonic circulation over the

261 SCS, known as the monsoon trough. This westerly monsoon flow transports a large amount

262 of water vapor to the SCS and leads to moisture convergence there associated with the

263 cyclonic flow, inducing convection and producing large precipitation in the region.

264 The general features of summer climatological precipitation, low-level wind and land-

265 sea contract of SLP are well reproduced by GOML2 model. However, the westerly from the

266 Indian Ocean is stronger in the model due to the overestimated meridional land-sea SLP

267 contrast. Thus, the westerly wind and monsoon trough extend eastward into the WNP in the

268 model and the simulated precipitation in the monsoon trough is larger than in observations.

269 Despite these biases, the model simulates the summer climatological precipitation and

270 low-level circulation over East Asia and adjacent regions well compared with observations,

271 which suggests this model can be an appropriate tool to study the precipitation change over

272 the SCS in response to different forcings.

273

274 **4 Model simulated changes in response to different forcings**

275 To explore the effects of anthropogenic forcing on the SCSSM in model experiments,

276 the changes in precipitation, low-level circulation and 500hPa vertical velocity in response

277 to changes in both GHG and AA forcings are shown in Fig.3a. Model simulated responses

278 to changes in anthropogenic forcing from EP to PD are characterized by anomalous

279   easterlies from the WNP, across the SCS, into the Indian peninsula, indicating a weakening

280   of climatological westerlies. The weakened westerlies are associated with reduced

281   precipitation in latitude band of (10°N-20°N) and increased precipitation to the south. These

282   features in the model simulations are similar to observed inter-decadal changes between

283   PD and EP in observations (Fig.1b), indicating that the changes in anthropogenic forcing

284   might have played a dominant role in the observed inter-decadal changes of the SCSSM

285   and reduced precipitation over the SCS in the late 20th century.

286   Shown in Fig.3 b and c are model simulated changes in response to either changes in

287   GHG or AA forcing. The patterns of large-scale circulation and precipitation in response to

288   changes in AA forcing (Fig. 3c) are similar to changes in ALL forcing experiment (Fig. 3a).

289   Although precipitation under GHG forcing reduces as well, the easterly anomaly over the

290   SCS region is weak. These responses to individual forcing change indicate that model

291   simulated weakening of the SCSSM and reduced precipitation over the SCS from EP to PD

292   are predominantly due to changes in AA forcing (Fig.3a, c) with weak contributions from

293   changes in GHG (Fig. 3b).

294   To investigate the processes that contribute to the precipitation changes in the model

295   simulated responses to different forcings, the column integrated moisture flux transports and

296   their convergences are shown in Fig.4. The moisture flux transports and their convergences

297   are further decomposed into a dynamic component due to circulation change and a

298   thermodynamic component due to humidity change (e.g., Li and Ting 2017, Tian et al. 2018).

299   In many aspects, the patterns of changes in moisture flux convergences and their

300   magnitudes in response to different forcings (Fig. 4a, d, g) are similar to changes in model

301   simulated precipitation responses (Fig. 3). This indicates that it is the moisture flux

302 convergence responsible for model simulated precipitation changes. However, changes in

303 dynamic components and thermodynamics components show some different features in

304 response to different forcings. In response to ALL forcing change, the dynamic components

305 (Fig.4b) show anomalous westward moisture flux transport and anomalous moisture

306 transport divergence from the WNP, across the SCS, into the SASM region. These

307 anomalies in dynamic components are partially offset by anomalous eastward moisture

308 transports and convergences due to thermodynamic components related to warming mainly

309 induced by changes in GHG (this will be discussed in section 5). In response to changes in

310 GHG forcing, the model simulated moisture convergence changes (Fig.4d) are weak over

311 the SCS due to compensation between the dynamic component related to weakened

312 circulation (Fig.4e) and thermodynamic component related to increased water vapor in the

313 atmosphere (Fig. 4f). In response to changes in AA forcing, the changes in moisture flux

314 transports and their divergences are predominantly due to dynamic components related to

315 circulation changes with weak contribution from changes in humidity (Fig. 4g, h, and i).

316 To quantify the regional precipitation changes over the SCS, area averaged precipitation

317 changes in observations and model simulated changes in response to different forcings are

318 shown in Figure 5a. ALL forcing change leads to a decrease in precipitation by 0.32mm/day

319 and contributes approximately 72% of observed inter-decadal decrease (-0.44mm/day),

320 suggesting anthropogenic forcing changes from EP to PD might have been a dominating

321 effect for observed inter-decadal decrease in precipitation in the late 20th century. Individual

322 forcing both have a positive contribution on precipitation decrease with a dominant

323 contribution from changes in AA forcings. The regional averaged moisture transport

324 convergence is shown in Figure 5c. As the total moisture transport convergence shows a

325 similar change as precipitation in Fig.5a, the dynamic and thermodynamic components

326 clearly show how anthropologic forcings change circulation and humidity, and contribute to

327 the interdecadal deceased precipitation. All forcing, GHG forcing and AA forcing result in

328 weakened dynamic moisture transport convergence. However, as GHG changes warm the

329 atmosphere significantly, the thermodynamic part of all forcing and GHG forcing increases

330 and this offsets the dynamic component partially. AA emission changes do not change the

331 humidity much, so the thermodynamic component in AA forcing is weak and the weakened

332 total moisture transport convergence is predominantly related to changes in circulation. It

333 should be noted a nonlinearity of changes in the SCSSM in response to changes in GHG

334 and AA emissions (i.e., the response to the combined forcings is not necessarily equal to

335 the sum of the responses to the individual forcings). In particular, the sum of precipitation

336 changes over the SCS in response to GHG and AA changes is larger than the change in

337 response to ALL forcing. The nonlinearity noticed in this study is consistent with some

338 previous studies (Feichter et al. 2004, Ming and Ramaswamy 2009, Shiogama et al. 2012).

339 However, detailed investigation of the causes in this nonlinearity is beyond the scope of this

340 study.

341   The regional averaged zonal wind components over southern SCS (5°N-15°N, 105°E-

342 120°E) are shown in Fig.5b. In observations and model experiments, zonal wind in this

343 region change most significantly. This figure further illustrates that the weakened

344 precipitation over the SCS in response to changes in anthropogenic forcing (ALL forcing) is

345 mainly contributed by the weakened zonal wind and reduced moisture transports, and the

346 response to AA forcing plays a dominant role. In summary, it has demonstrated that the

347 circulation and precipitation changes in response to changes in individual GHG or AA forcing

348 show different characteristics. Thus, in the next two sections, we are exploring physical

349 processes that are responsible for the large-scale circulation differences in response to

350 individual forcing respectively.

351

352 **5 Mechanism related to GHG forcing**

353 The model simulated precipitation changes under GHG forcing show some weak

354 decreases, mainly resulted from the moisture flux transport compensation between the

355 dynamic component related to weakened circulation and thermodynamic component related

356 to increased humidity. What processes are responsible for the circulation and humidity

357 changes in the model simulations?

358 In GHG forcing experiment, large scale anomalous descends cover a large area

359 including the SASM region and the SCS region, accompanied by a low-level easterly

360 anomaly (Fig.3b). These anomalous local circulation anomalies and descents are

361 associated with anomalous large-scale divergent circulations in the tropical Indian and

362 Pacific oceans (Fig. 6). These anomalous large-scale circulations indicate anomalous

363 convergence over the tropical eastern Pacific in the lower troposphere and anomalous

364 divergence in the upper troposphere with opposite changes over the tropical Indian ocean

365 and the western tropical Pacific, being associated with weakened Walker circulation.

366 Associated with these large-scale divergent circulations are that SST warming is stronger in

367 the eastern tropical Pacific (over 0.5℃) than western tropical Pacific (about 0.3℃) (Fig.7b),

368 indicating a weakening zonal SST gradient in the tropical Pacific. This association between

369 the change in zonal SST gradient and large scale divergent circulations is consistent with

370 previous researches which suggested that the zonal SSTA gradient change associated with

371   El-Nino like SST anomalies enhances convection over the eastern equatorial Pacific and

372   leads to a weakened Walker circulation over the tropics (Ju and Slingo 1995; Timmermann

373   et al. 1999; Wilhelm, 2002).

374   How do changes in GHG forcing lead to enhanced warming over the eastern tropical

375   Pacific than in western tropical Pacific?　Firstly, GHG forcing changes surface radiation

376   balance. With increase in GHG forcing, both clear sky surface longwave radiation (clear-sky

377   LW) and surface longwave cloud radiative effect (CRE-LW) increase over the equatorial

378   Pacific (Fig.7c and 7d). Because mixed layer depth is deeper in the western tropical Pacific

379   than in the eastern tropical Pacific, the response of SSTA is weaker in the west and stronger

380   in the east. This zonal asymmetry leads to a weakened zonal SST gradient and Walker

381   circulation through the dynamic processes elucidated above. This mechanism agrees with

382   previous research (DiNezio et al. 2009; Yeh et al. 2009; Collins et al. 2010) which revealed

383   the relationship of climate change, El-Nino like SSTA change and relative trade wind change.

384   Secondly, as air temperature increases due to increasing GHG concentrations, atmosphere

385   can hold more moisture over the SCS. Warmer sea surface temperature can also increase

386   the evaporation locally so both these changes lead to increase in the water vapor in the

387   atmosphere (Fig.7a).

388   The results above indicate that the decreasing precipitation and weakened monsoon

389   circulation over the SCS in GHG forcing experiments are caused by anomalous descend

390   which is related to weakened Walker circulation.

391

392   **6 Mechanism related to AA forcing**

393   In response to changes in AA forcing, the changes in moisture flux transports and their

394   divergences are predominantly due to dynamic components related to circulation changes

395   with weak contribution from changes in humidity (Fig. 4g, h, i). In AA forcing experiment,

396   there are significant easterly anomalies over the monsoon region from the Arabian Sea to

397   the western North Pacific (Fig. 3c).

398   To understand the mechanism of these circulation changes, we analyze the zonal mean

399   (60°E-150°E) meridional overturning circulation changes in response to AA forcing (Fig.8a).

400   These anomalous overturning circulations are characterized by anomalous descents around

401   monsoon region (10°N-25°N) and anomalous ascends around the equator, indicating a

402   change in local Hadley circulation. Previous researches suggest that this anomalous local

403   Hadley circulation might be a result of SSTA meridional gradient (Ganguly et al. 2012;

404   Ganguly et al. 2012; Ramanathan et al. 2005; Chung et al. 2006; Luo et al. 2019). However,

405   the SSTA gradient change in JJA is weak in response to AA forcing (Fig. 8b). The SSTA

406   over ascend region is about -0.05℃ and it is about 0℃ over descend region (Fig8b). This

407   association between anomalous ascents (descents) with anomalous cold (weak) SST

408   seems counterintuitive. However, this simultaneous association includes atmospheric

409   feedbacks on SST changes. Thus, we explore the SSTA in pre-monsoon seasons (Fig.9).

410   There is no significant SSTA over the northern Indian Ocean (NIO) and the SCS in JJA, but

411   during December to February (DJF) and March to May (MAM), SST is cooled to the north

412   of the equator in this region (about -0.1℃ to -0.3℃). This meridional SST gradient in pre-

413   monsoon seasons is key processes for local Hadley circulation anomaly in JJA.

414   To understand the process of how aerosol changes affect SSTA and circulation in the

415   pre-monsoon seasons, seasonal evolutions of zonal averaged changes over the monsoon

416   region (60°E-150°E) are analyzed and they are illustrated in Fig. 10. Results indicate that

417   large summer monsoon precipitation and circulation changes occur in June and become

418   weaker in July and August (Fig.10a and 10b). The meridional SSTA gradient with relative

419   large cold anomalies of about 0.2℃ in the northern subtropics sustains during pre-monsoon

420   seasons until it gets weaker after May and June when monsoon establishes (Fig.10c). This

421   SSTA pattern and associated meridional SST gradient (cooler in north than in south)

422   sustains until May and June when it drives a local Hadley circulation which causes an

423   anomalous descend over monsoon region and then weakened westerly low-level flow and

424   less precipitation.

425   This SSTA annual cycle is driven by surface radiation changes. In response to AA

426   forcing, clear-sky surface shortwave radiation (clear-sky SW) decreases all year round over

427   the ocean with maximum changes during SON and MAM (Fig.10d), which cause a cooler

428   SSTA locally. The clear-sky SW changes are closely related to the aerosol-radiation

429   interaction and aerosol-cloud interaction. Changes in aerosol optical depth (AOD), cloud

430   droplet effective radius (CDER) and cloud droplet number (CDN) are larger over the NIO

431   and the SCS in pre-monsoon seasons (largest during SON) than in JJA since aerosol

432   emissions are advected by the prevailing winds   to these regions (Fig.11j-11i). These

433   changes are characterized by increases in AOD, decreases in CDER, and increases in CDN.

434   Note that seasonal changes in CDER show some differences in comparison with changes

435   in AOD and CDN since CDER-CDN relationship is not linear (Jones et al. 2001) and CDER

436   change is more sensitive to the basic state environment than CDN over ocean where the

437   atmosphere is cleaner (Carslaw et al. 2013). These changes in AOD, CDN, and CDER are

438   responsible for the seasonal evolutions of changes in surface clear sky SW and SST (Fig.

439   10c, d).   As a result, the SSTA is cool over the NIO to equatorial IO since SON and sustains

440   until May and Jun.

441   In May and June, the SST is still cooler over the NIO than around the equator, which

442   drives a local Hadley circulation. However, upward surface latent heat flux reduces related

443   to weakened low-level westerlies (anomalous easterlies) over monsoon region (positive

444   downward in Fig.10e). Meanwhile shortwave cloud radiative effect shows positive changes

445   (CRE-SW, Fig.10f) due to less cloud cover associated with reduced convection. These

446   feedbacks associated with the changes in circulation and surface radiation damp cold SST

447   anomalies induced by AA change in pre-monsoon seasons, leading to weak SST anomalies

448   in JJA and weak meridional SST gradient.

449   In summary, when changes in AA emissions are advected by prevailing winds from the

450   Asian continent to the NIO and the SCS in pre-monsoon seasons, the SST is cooled by

451   reduced clear sky SW while changes in both clear sky SW radiation and SST are weak in

452   the southern hemisphere. These result in anomalous meridional SST gradient in Asian

453   sector and this meridional SST gradient sustains until boreal summer, which in turn drives

454   weakened monsoon circulation and precipitation over the SCS in summer. In May and June

455   when precipitation is reduced, the SST warms over the NIO due to increased shortwave

456   cloud radiative effect (Fig. 10f) related to reduced cloud cover and weakened latent heat flux

457   (Fig. 10e) related to weakened westerlies. These processes tend to damp cold SST

458   anomalies in pre-monsoon seasons lead to weak summer mean SST anomalies over the

459   NIO (Fig.9d, Fig. 10c).

460

461   7 Conclusion and discussion

462   Base on observations, there is a significant inter-decadal decrease of precipitation over

463   the SCS between 1964-1981 and 1994-2011 during boreal summer monsoon season (JJA).

464   Corresponding to the change in precipitation is a weakened SCSSM circulation,

465   characterized by anomalous descend over the SCS, weaker westerly monsoon flow in the

466   lower troposphere and less moisture flux transport convergence to the SCSSM region. In

467   this study, a set of experiments based on MetUM-GOML2 model is used to investigate the

468   role of anthropogenic forcing (including GHG and AA emission) changes and quantify the

469   relative roles of GHG and AA forcing, on the inter-decadal decrease of the SCSSM and

470   precipitation.   The main results are summarized as follows:

471   1.   Model results suggest that the changes in anthropogenic forcing from EP (1964-

472   1981) to PD (1994-2011) might have played a dominant role in the observed inter-decadal

473   changes of the SCSSM and reduced precipitation in the late 20th century in which AA forcing

474   plays a more important role compared with GHG forcing.

475   2.   Increased GHG concentrations lead to positive changes in surface longwave

476   radiation over the tropical Pacific. Due to the asymmetric mixed layer depth, warming in the

477   eastern equatorial Pacific is greater than in the western tropical Pacific. This El-Niño-like

478   SSTA pattern leads to a weaker Walker circulation and causes a large-scale descend in

479   both Indian monsoon and SCS monsoon region, and causes a weaker westerly low-level

480   flow. This weakened monsoon circulation leads to weakened moisture flux transport

481   convergence and therefore reduced precipitation over the SCS. Meanwhile, the warm SST

482   anomalies lead to increases of evaporation and the water vapor in the atmosphere. This

483   leads to increased moisture flux transport convergence and therefore enhanced

484   precipitation over the SCS. Due to this compensation between dynamical moisture transport

485   and thermodynamic moisture transport, the changes in moisture transport convergence, and

486 therefore precipitation over the SCS are weak.

487 3. In response to changes in AA emissions, CDN and AOD increase while CDER

488 decreases over continental Asia due to increased AA emissions over Asia. In pre-monsoon

489 seasons, aerosol emissions are transported to the northern Indian Ocean and the SCS by

490 prevailing winds, leading to increases in CDN and AOD and decreases in CDER in these

491 regions. These changes lead to reduced surface clear-sky shortwave radiation in the

492 northern subtropics with weak changes in southern hemisphere. As a result, the SST in the

493 northern subtropics decreases by about 0.2℃ in pre-monsoon seasons and this cold

494 anomaly sustains until the establishment of summer monsoon. This nonuniform SST change

495 leads to a meridional SST gradient which in turn induces a local Hadley circulation change

496 with anomalous descending at monsoon region and the anomalous easterly wind in the

497 lower troposphere which transport less moisture to the SCS monsoon region, leading to

498 reduced precipitation.

499 Our modelling results suggest that changes in GHG concentrations and AA emissions

500 might have played an important role in decreased SCSSM and reduced precipitation on the

501 SCS in the late 20th century in which AA forcing plays a more important role compared with

502 GHG forcing. This result is in agreement to some previous researches about role of AA

503 changes in the East Asian summer monsoon based on CMIP5 models (Song et al. 2014;

504 Zhang and Li 2016) .

505 Although the observed inter-decadal decrease of SCSSM precipitation can be captured

506 by this model, it should be pointed out that these results and processes are based on this

507 specific model and experiment design. For example, these experiments use GHG and AA

508 forcing of two specific periods (1964-1981 and 1994-2011) and the ocean model is a mixed

509   layer model. Therefore, the role of ocean dynamics are not included in our experiments. In

510   the future, the reliability of the physical processes in this study can be tested by comparing

511   with other models' results which consider the oceanic circulation changes in response to

512   different forcings. In addition, it should be noted a nonlinearity of changes in the SCSSM in

513   response to changes in GHG and AA emissions (i.e., the response to the combined forcings

514   is not necessarily equal to the sum of the responses to the individual forcings). The

515   nonlinearity noticed in this study is consistent with some previous studies (Feichter et al.

516   2004, Ming and Ramaswamy 2009, Shiogama et al. 2012), and needs to be investigated

517   further.

518

527

528
529

530 Reference:

531 Adler RF, Huffman GJ, Chang A, et al (2003) The Version-2 Global Precipitation Climatology

532   Project (GPCP) Monthly Precipitation Analysis (1979–Present). J Hydrometeorol. doi:

533   10.1175/1525-7541(2003)004<1147:tvgpcp>2.0.co;2

534 Allan R, Ansell T (2006) A new globally complete monthly historical gridded mean sea level

535   pressure dataset (HadSLP2): 1850-2004. J Clim. doi: 10.1175/JCLI3937.1

536 Bellouin N, Mann GW, Woodhouse MT, et al (2013) Impact of the modal aerosol scheme

537   GLOMAP-mode on aerosol forcing in the hadley centre global environmental model.

538   Atmos Chem Phys. doi: 10.5194/acp-13-3027-2013

539 Bellouin N, Rae J, Jones A, et al (2011) Aerosol forcing in the Climate Model

540   Intercomparison Project (CMIP5) simulations by HadGEM2-ES and the role of

541   ammonium nitrate. J Geophys Res Atmos. doi: 10.1029/2011JD016074

542 Bollasina MA, Ming Y, Ramaswamy V (2011) Anthropogenic Aerosols and the Summer

543   Monsoon. Science (80-) 334:502–505

544 Boucher O, Randall D, Artaxo P, Bretherton C, Feingold G, Forster P, Zhang X (2013)

545   Clouds and aerosols. In: Stocker T et al (eds) Climate change 2013: the physical

546   science basis. Contribution of working group I to the fifth assessment report of the

547   intergovernmental panel on climate change. Cambridge University Press, Cambridge,

548   pp 571–657

549 Carslaw KS, Lee LA, Reddington CL, Pringle KJ, Rap A, Forster PM, Mann GW, Spracklen

550   DV, Woodhouse MT, Regayre LA, Pierce JR (2013) Large contribution of natural

551   aerosols to uncertainty in indirect forcing. Nature 503:67–71

552 Charlson RJ, Schwartz SE, Hales JM, et al (1992) Climate forcing by anthropogenic

553   aerosols. Science (80-). doi: 10.1126/science.255.5043.423

554 Chen L and O. W. Frauenfeld (2016) A comprehensive evaluation of precipitation

555   simulations over China based on CMIP5 multimodel ensemble projections. J Geophys

556   Res Atmos 121:5430–5452. doi: 10.1002/2013JD021190.Received

557 Chen M, Xie P, Janowiak JE, Arkin PA (2002) Global Land Precipitation: A 50-yr Monthly
558   Analysis Based on Gauge Observations. J Hydrometeorol. doi: 10.1175/1525-
559   7541(2002)003<0249:glpaym>2.0.co;2

560 Chen W, and Dong B (2019) Anthropogenic impacts on recent decadal change in
561   temperature extremes over China: Relative roles of greenhouse gases and
562   anthropogenic aerosols. *Climate Dyn.* 52, 3643–3660, doi: 10.1007/s00382-018-4342-
563   9.

564 Chung CE, Ramanathan V (2006) Weakening of north Indian SST gradients and the
565   monsoon rainfall in India and the Sahel. J Clim. doi: 10.1175/JCLI3820.1

566 Collins M, An S II, Cai W, et al (2010) The impact of global warming on the tropical Pacific
567   Ocean and El Nĭo. Nat Geosci 3:391–397. doi: 10.1038/ngeo868

568 Dai N, Xie A, Zhang Y (2000) Interannual and Interdecadal Variations of Summer Monsoon
569   Activities over South China Sea[J]. Climatic and Environmental Research(in
570   Chinese),5(4):363-374,doi:10.3878/j.issn.1006-9585.2000.04.04.

571 Ding Y (1992) Summer monsoon rainfall in China. J. Meteorol. Soc. Jpn. 70, 373–396

572 Ding Y, Sun Y, Wang Z, et al (2009) Inter-decadal variation of the summer precipitation in
573   China and its association with decreasing Asian summer monsoon Part II: Possible
574   causes. Int J Climatol 29:1926–1944. doi: 10.1002/joc.1759

575 Ding Y, Wang Z, Sun Y (2008) Inter-decadal variation of the summer precipitation in East
576   China and its association with decreasing Asian summer monsoon. Part I: Observed
577   evidences. Int J Climatol. doi: 10.1002/joc.1615

578 DiNezio PN, Clement AC, Vecchi GA, et al (2009) Climate response of the equatorial pacific
579   to global warming. J Clim 22:4873–4892. doi: 10.1175/2009JCLI2982.1

580 Dong B, Gregory JM, Sutton RT (2009) Undestanding land-sea warming contrast in
581   response to increasing greenhouse gases. Part I: Transient adjustment. J Clim

582   22:3079–3097. doi: 10.1175/2009JCLI2652.1

583 Dong B, Sutton RT, Highwood EJ, Wilcox LJ (2016) Preferred response of the East Asian
584   summer monsoon to local and non-local anthropogenic sulphur dioxide emissions. Clim
585   Dyn 46:1733–1751. doi: 10.1007/s00382-015-2671-5

586 Feichter J, Roeckner E, Lohmann U, Liepert B (2004) Nonlinear aspects of the climate
587   response to greenhouse gas and aerosol forcing. J Clim 17:2384–2398

588 Ganguly D, Rasch PJ, Wang H, Yoon JH (2012a) Fast and slow responses of the South
589   Asian monsoon system to anthropogenic aerosols. Geophys Res Lett 39:1–5. doi:
590   10.1029/2012GL053043

591 Ganguly D, Rasch PJ, Wang H, Yoon JH (2012b) Climate response of the South Asian
592   monsoon system to anthropogenic aerosols. J Geophys Res Atmos 117:1–20. doi:
593   10.1029/2012JD017508

594 Goswami B, Madhusoodanan M, Neema C, Sengupta D (2006) A physical mechanism for
595   North Atlantic SST influence on the Indian summer monsoon. Geophys Res Lett 33,
596   L02706. doi: 10.1029/2005GL024803

597 Guo L, Highwood EJ, Shaffrey LC, Turner AG (2013) The effect of regional changes in
598   anthropogenic aerosols on rainfall of the East Asian Summer Monsoon. Atmos Chem
599   Phys. doi: 10.5194/acp-13-1521-2013

600 Held IM, Soden BJ (2006) Robust responses of the hydrologic cycle to global warming. J
601   Clim. doi: 10.1175/JCLI3990.1

602 Hu ZZ, Latif M, Roeckner E, Bengtsson L (2000) Intensified Asian summer monsoon and its
603   variability in a coupled model forced by increasing greenhouse gas concentrations.
604   Geophys Res Lett 27:2681–2684. doi: 10.1029/2000GL011550

605 JIANG D and Wang H (2005) Natural interdecadal weakening of East Asian summer
606   monsoon in the late 20th century. Chinese Sci Bull 50:1923. doi: 10.1360/982005-36

607 Jones A, Roberts DL, Woodage MJ, Johnson CE (2001) Indirect sulphate aerosol forcing in

608   a climate model with an interactive sulphur cycle. J Geophys Res 106 D17: 20,293–

609   20,310

610 Jones CD, Hughes JK, Bellouin N, et al (2011) The HadGEM2-ES implementation of CMIP5

611   centennial simulations. Geosci Model Dev. doi: 10.5194/gmd-4-543-2011

612 Ju J, Slingo J (1995) The Asian summer monsoon and ENSO. Q J R Meteorol Soc. doi:

613   10.1002/qj.49712152509

614 Kalnay E, Kanamitsu M, Kistler R, et al (1996) The NCEP/NCAR 40-year reanalysis project.

615   Bull Am Meteorol Soc. doi: 10.1175/1520-0477(1996)077<0437:TNYRP>2.0.CO;2

616 Lamarque JF, Bond TC, Eyring V, et al (2010) Historical (1850-2000) gridded anthropogenic

617   and biomass burning emissions of reactive gases and aerosols: Methodology and

618   application. Atmos Chem Phys. doi: 10.5194/acp-10-7017-2010

619 Lau NC, Ann MJ, Wang H (2005). Simulations by a GFDL GCM of ENSO-related variability

620   of the coupled atmosphere-ocean system in the East Asian Monsoon region. East Asian

621   Monsoon.

622 Lau NC., Wang B. (2006) Interactions between the Asian monsoon and the El Niño/Southern

623   Oscillation. In: The Asian Monsoon. Springer Praxis Books. Springer, Berlin, Heidelberg

624 Lau KM, Kim KM (2017) Competing influences of greenhouse warming and aerosols on

625   Asian summer monsoon circulation and rainfall. Asia-Pacific J Atmos Sci 53:181–194.

626   doi: 10.1007/s13143-017-0033-4

627 Lau KM, Yang S (1997) Climatology and interannual variability of the Southeast Asian

628   summer monsoon. Adv Atmos Sci. doi: 10.1007/s00376-997-0016-y

629 Lee SM, Jhun JG, Kwon M, Kim W (2008) Change in the western North Pacific summer

630   monsoon circulation due to the CO_2 increase in IPCC AR4 CGCMs. Asia Pac J Atmos

631   Sci 44(4):351–368

632 Levine RC, Turner AG, Marathayil D, Martin GM (2013) The role of northern Arabian Sea

633   surface temperature biases in CMIP5 model simulations and future projections of Indian

summer monsoon rainfall. Clim Dyn 41:155–172. doi: 10.1007/s00382-012-1656-x

Li C, and Zhang L, (1999) Summer monsoon activities in the South China Sea and its impacts. Chin. J. Atmos. Sci., 23, 257–266.

Li G, Xie SP (2012) Origins of tropical-wide SST biases in CMIP multi-model ensembles. Geophys Res Lett 39:1–5. doi: 10.1029/2012GL053777

Li G, Xie SP, Du Y (2015) Monsoon-induced biases of climate models over the tropical Indian Ocean. J Clim 28:3058–3072. doi: 10.1175/JCLI-D-14-00740.1

Li J, Wu Z, Jiang Z, He J (2010) Can global warming strengthen the East Asian summer monsoon? J Clim. doi: 10.1175/2010JCLI3434.1

Li X, Ting M (2017) Understanding the Asian summer monsoon response to greenhouse warming: the relative roles of direct radiative forcing and sea surface temperature change. Clim Dyn. doi: 10.1007/s00382-016-3470-3

Li X, Ting M, Li C, Henderson N (2015) Mechanisms of Asian Summer Monsoon Changes in Response to Anthropogenic Forcing in CMIP5 Models*. J Clim. doi: 10.1175/jcli-d-14-00559.1

Li Z, Lau WKM, Ramanathan V, et al (2016) Aerosol and monsoon climate interactions over Asia. Rev. Geophys.

Liang J, Wu S, and You J, (1999) The research on variations of onset time of the SCS summer monsoon and its intensity. Chin. J. Trop. Meteor., 15, 97–105.

Lu E. and Chan J, (1999) A Unified Monsoon Index for South China. J. Climate, 12, 2375–2385, doi: 10.1175/1520-0442(1999)012<2375:AUMIFS>2.0.CO;2

Lu R, Dong B, Ding H (2006) Impact of the Atlantic Multidecadal Oscillation on the Asian summer monsoon. Geophys Res Lett 33:1–5. doi: 10.1029/2006GL027655

Luo F, Dong B, Tian F, Li S (2019) Anthropogenically Forced Decadal Change of South Asian Summer Monsoon Across the Mid-1990s. J Geophys Res Atmos 124:806–824. doi: 10.1029/2018JD029195

660   Murakami T., Matsumoto J. (1994). Summer monsoon over the Asian continent and western
661   north Pacific. J. Meteorol. Soc. Jpn. 72, 719–745.

662   May W (2002) Simulated changes of the Indian summer monsoon under enhanced
663   greenhouse gas conditions in a global time-slice experiment. Geophys Res Lett. doi:
664   10.1029/2001GL013808

665   Menon S, Hansen J, Nazarenko L (2002) Climate Effects of Black Carbon Aerosols in China
666   and India. 297:2250–2254

667   Ming Y, Ramaswamy V (2009) Nonlinear climate and hydrological responses to aerosol
668   effects. J Clim 22:1329–1339

669   Ming Y, Ramaswamy V, Persad G (2010) Two opposing effects of absorbing aerosols on
670   global-mean precipitation. Geophys Res Lett 37:1–4. doi: 10.1029/2010GL042895

671   Ming Y, Ramaswamy V (2011) A model investigation of Aerosol-Induced changes in tropical
672   circulation. J Clim. doi: 10.1175/2011JCLI4108.1

673   Pitari G, Ackerman A, Adams P, et al (2001) Aerosols, their Direct and Indirect Effects. Clim
674   Chang 2001 Sci Basis Contrib Work Gr I to Third Assess Rep Intergov Panel Clim
675   Chang 5:289–348

676   Prell WL (2011) Variation of monsoonal upwelling: A response to changing solar radiation

677   Ramanathan V, Chung C, Kim D, et al (2005) Atmospheric brown clouds: Impacts on South
678   Asian climate and hydrological cycle. Proc Natl Acad Sci. doi:
679   10.1073/pnas.0500656102

680   Ramanathan V, Crutzen PJ, Kiehl JT, Rosenfeld D (2001) Atmosphere: Aerosols, climate,
681   and the hydrological cycle. Science (80-) 294:2119 – 2124. doi:
682   10.1126/science.1064034

683   Rotstayn LD, Lohmann U (2002) Tropical rainfall trends and the indirect aerosol effect. J
684   Clim. doi: 10.1175/1520-0442(2002)015<2103:TRTATI>2.0.CO;2

685   Seo KH, Ok J, Son JH, Cha DH (2013) Assessing future changes in the East Asian summer

686   monsoon using CMIP5 coupled models. J Clim 26:7662–7675. doi: 10.1175/JCLI-D-12-
687   00694.1

688 Sharmila S, Joseph S, Sahai AK, et al (2015) Future projection of Indian summer monsoon
689   variability under climate change scenario: An assessment from CMIP5 climate models.
690   Glob Planet Change 124:62–78. doi: 10.1016/j.gloplacha.2014.11.004

691 Shiogama H, Stone DA, Nagashima T, Nozawa T, Emori S (2012) On the linear additivity of
692   climate forcing-response relationships at global and continental scales Int. J Climatol
693   33:2542–2550

694 Smith DM, Murphy JM (2007) An objective ocean temperature and salinity analysis using
695   covariances from a global climate model. J Geophys Res Ocean. doi:
696   10.1029/2005JC003172

697 Song F, Zhou T, Qian Y (2014) Responses of East Asian summer monsoon to natural and
698   anthropogenic forcings in the 17 latest CMIP5 models. Geophys Res Lett. doi:
699   10.1002/2013GL058705

700 Sun Y, Ding Y, Dai A (2010) Changing links between South Asian summer monsoon
701   circulation and tropospheric land-sea thermal contrasts under a warming scenario.
702   Geophys Res Lett 37:1–5. doi: 10.1029/2009GL041662

703 Sutton RT, Dong B, Gregory JM (2007) Land/sea warming ratio in response to climate
704   change: IPCC AR4 model results and comparison with observations. Geophys Res Lett
705   34:2–6. doi: 10.1029/2006GL028164

706 Tanaka HL, Ishizaki N, Kitoh A (2004) Trend and interannual variability of Walker, monsoon
707   and Hadley circulations defined by velocity potential in the upper troposphere. Tellus,
708   Ser A Dyn Meteorol Oceanogr 56:250–269. doi: 10.1111/j.1600-0870.2004.00049.x

709 Tao S, Chen L. (1987) A review of recent research on the East Asian summer monsoon in
710   China. In:Chang,C.-P.,Krishnamurti, T.N. (Eds.), Monsoon Meteorology. Oxford
711   University Press, New York, pp. 60–92.

712 Tian F, Dong B, Robson J, Sutton R (2018) Forced decadal changes in the East Asian
713   summer monsoon: the roles of greenhouse gases and anthropogenic aerosols. Clim
714   Dyn 51:3699–3715. doi: 10.1007/s00382-018-4105-7

715 Timmermann A, Oberhuber J, Bacher A, et al (1999) Increased El Nino frequency in a
716   climate model forced by future greenhouse warming. Nature. doi: 10.1038/19505

717 Tong HW, Chan JCL, Zhou W (2009) The role of MJO and mid-latitude fronts in the South
718   China Sea summer monsoon onset. Clim Dyn 33:827–841. doi: 10.1007/s00382-008-
719   0490-7

720 Trenberth KE, Shea DJ (2006) Atlantic hurricanes and natural variability in 2005. Geophys
721   Res Lett 33:1–4. doi: 10.1029/2006GL026894

722 Ueda H, Iwai A, Kuwako K, Hori ME (2006) Impact of anthropogenic forcing on the Asian
723   summer monsoon as simulated by eight GCMs. Geophys Res Lett 33:20–23. doi:
724   10.1029/2005GL025336

725 Vecchi GA, Soden BJ (2007) Global warming and the weakening of the tropical circulation.
726   J Clim. doi: 10.1175/JCLI4258.1

727 Walters D, Boutle I, Brooks M, et al (2017) The Met Office Unified Model Global Atmosphere
728   6.0/6.1 and JULES Global Land 6.0/6.1 configurations. Geosci Model Dev. doi:
729   10.5194/gmd-10-1487-2017

730 Wang B, Huang F, Wu Z, et al (2009) Multi-scale climate variability of the South China Sea
731   monsoon: A review. Dyn. Atmos. Ocean.

732 Wang Z. & Qian Y. (2009) The relationship of land-ocean thermal anomaly difference with
733   mei-yu and South China Sea summer monsoon Adv. Atmos. Sci. 26: 169. doi:
734   10.1007/s00376-009-0169-y

735 Wang B, Yim SY, Lee JY, et al (2014) Future change of Asian-Australian monsoon under
736   RCP 4.5 anthropogenic warming scenario. Clim Dyn. doi: 10.1007/s00382-013-1769-x

737 Wang B, Zhang Q (2002) Pacific-East Asian teleconnection. Part II: How the Philippine Sea

738   anomalous anticyclone is established during El Niño development. J Clim. doi:
739   10.1175/1520-0442(2002)015<3252:PEATPI>2.0.CO;2

740   Wang C (2004) A modeling study on the climate impacts of black carbon aerosols. J
741   Geophys Res Atmos. doi: 10.1029/2003jd004084

742   Wen Z, Huang R, He H, and Lan G (2006) The influences of anomalous atmospheric
743   circulation over mid-high latitudes and the activities of 30-60d low frequency convection
744   over low latitudes on the onset of the South China Sea summer monsoon. Chin. J.
745   Atmos. Sci., 30, 952–964.

746   Wu G, Liu Y, He B, et al (2012) Thermal controls on the asian summer monsoon. Sci Rep
747   2:1–7. doi: 10.1038/srep00404

748   Wu S, and Liang J (2001) An index of South China Sea summer monsoon intensity and its
749   characters. Chin. J. Trop. Meteor., 17, 337–344.

750   Xie X, Wang H, Liu X, et al (2016), Distinct effects of anthropogenic aerosols on the East
751   Asian summer monsoon between multidecadal strong and weak monsoon stages, J.
752   Geophys. Res. Atmos., 121, 7026– 7040, doi:10.1002/2015JD024228.

753   Yao Y, and Qian Y (2001) A study on the South China Sea monsoon index and the
754   relationship between the index and regional rainfalls of China. J. Nanjing Uni., 37, 781–
755   788

756   Ye J, Li W, Li L, Zhang F (2013) "North drying and south wetting" summer precipitation
757   trend over China and its potential linkage with aerosol loading. Atmos Res 125–126:12–
758   19. doi: 10.1016/j.atmosres.2013.01.007

759   Yeh SW, Kug JS, Dewitte B, et al (2009) El Nĭo in a changing climate. Nature 461:511–514.
760   doi: 10.1038/nature08316

761   Zhang L, Li T (2016) Relative roles of anthropogenic aerosols and greenhouse gases in land
762   and oceanic monsoon changes during past 156 years in CMIP5 models. Geophys Res
763   Lett. doi: 10.1002/2016GL069282

764   Zhou T, Gong D, Li J, Li B (2009) Detecting and understanding the multi-decadal variability

765   of the East Asian Summer Monsoon – Recent progress and state of affairs, Meteorol.

766   Z., 18, 455–467.

767   Zhou W, Chan JCL (2005) Intraseasonal oscillations and the South China Sea summer

768   monsoon onset. Int J Climatol 25:1585–1609. doi: 10.1002/joc.1209

769   Zhou W, Chan JCL. ENSO and the South China Sea summer monsoon onset[J].

770   International Journal of Climatology, 2010, 27(2):157-167. doi：10.1002/joc.1380

771   Zhu Y, Wang H, Zhou W, Ma J (2011) Recent changes in the summer precipitation pattern

772   in East China and the background circulation. Clim Dyn 36:1463 – 1473. doi:

773   10.1007/s00382-010-0852-9

774   Table 1 Summarize of numerical experiments

775

Experiment		Ocean	Radiative Forcing
E0	Relaxation run	Relax to PD mean 3D ocean temperature and salinity to diagnose climatological temperature and salinity flux correction	Climatological PD (1994-2011) greenhouse gases (GHG) and anthropogenic aerosol (AA) precursor emissions. The GHG and AA forcing after 2006 are from RCP4.5 scenario
EP	Early period experiment	climatological temperature and salinity flux corrections from relaxation run	Climatological EP GHG (1964-1981) and EP AA(1970-1981) precursor emissions
PD-ALL	Present day all forcing experiment	same as above	Climatological PD GHG and PD AA precursor emissions
PD-GHG	Present day GHG forcing	same as above	Climatological PD GHG and EP AA precursor emissions
PD-AA	Present day AA forcing	same as above	Climatological EP GHG and PD AA precursor emissions

776

777

778
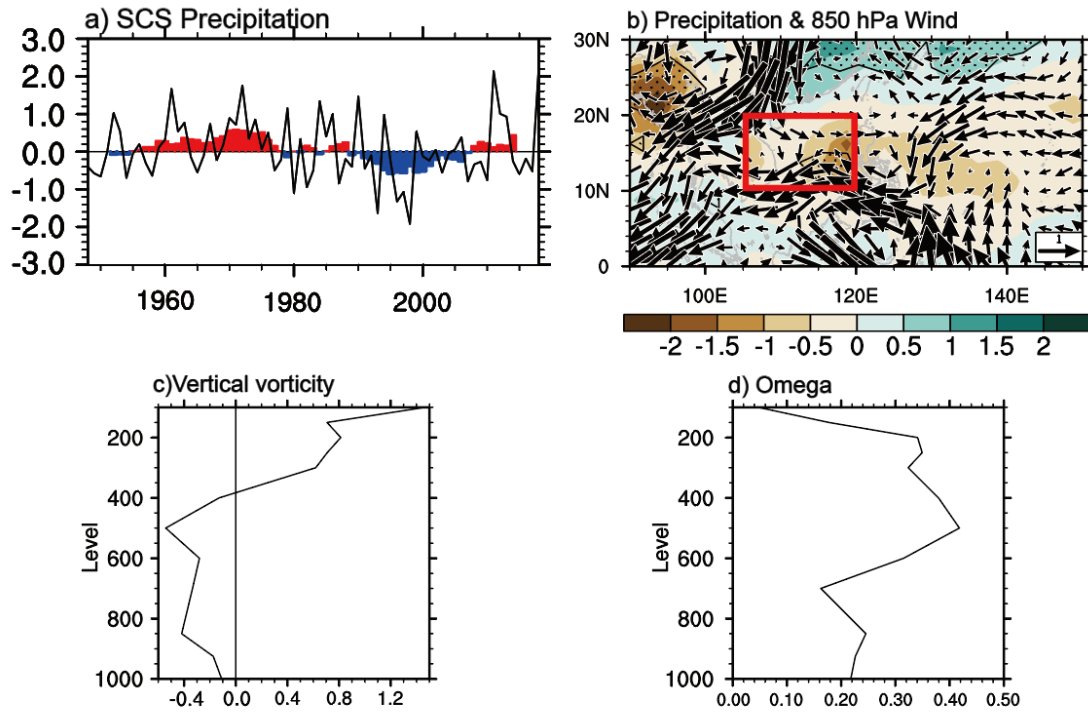
Fig.1 a) Time series (line) and 9 years moving mean (color bar) of (June-July-August) JJA

mean precipitation (mm day^{-1}) over the South China Sea region (10°N-20°N,105°E-120°E)

based on NOAA_PREC data set. b)-d) changes between present day (1994-2011) and

early period (1964-1981).

b) Precipitation (mm/day) of NOAA_PREC and 850hPa wind(m/s) of NCEP reanalysis.

Changes of precipitation in slash regions are statistically significant at the 10% level using

a two-tailed Student's t-test.

c) Vertical profile of vorticity (10^{-6}/s) over the SCS region, d) profile of vertical velocity

(Omega, hPa/s) in pressure coordinate over the SCS. Red box highlights the SCS region.

788

789
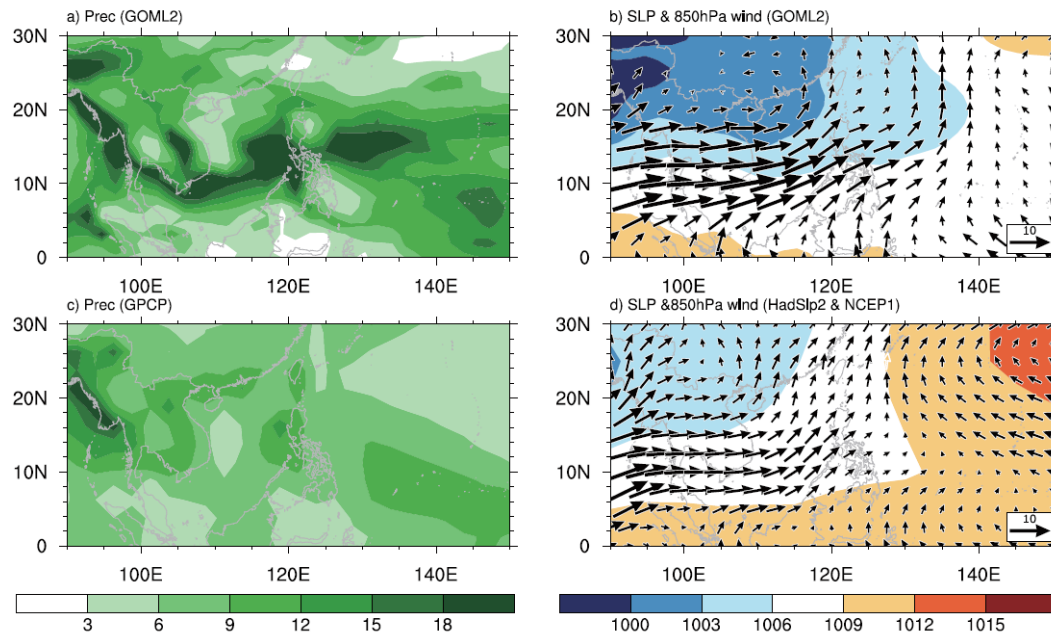
Fig.2 Present day (1994-2011) climatological precipitation (mm/day), sea level pressure

(hPa), and 850hPa wind(m/s) in JJA. a) and b) GOML2 simulation.

c) and d) GPCP precipitation, HadSLP2 SLP, and NCEP reanalysis 850 hPa wind.

793

794
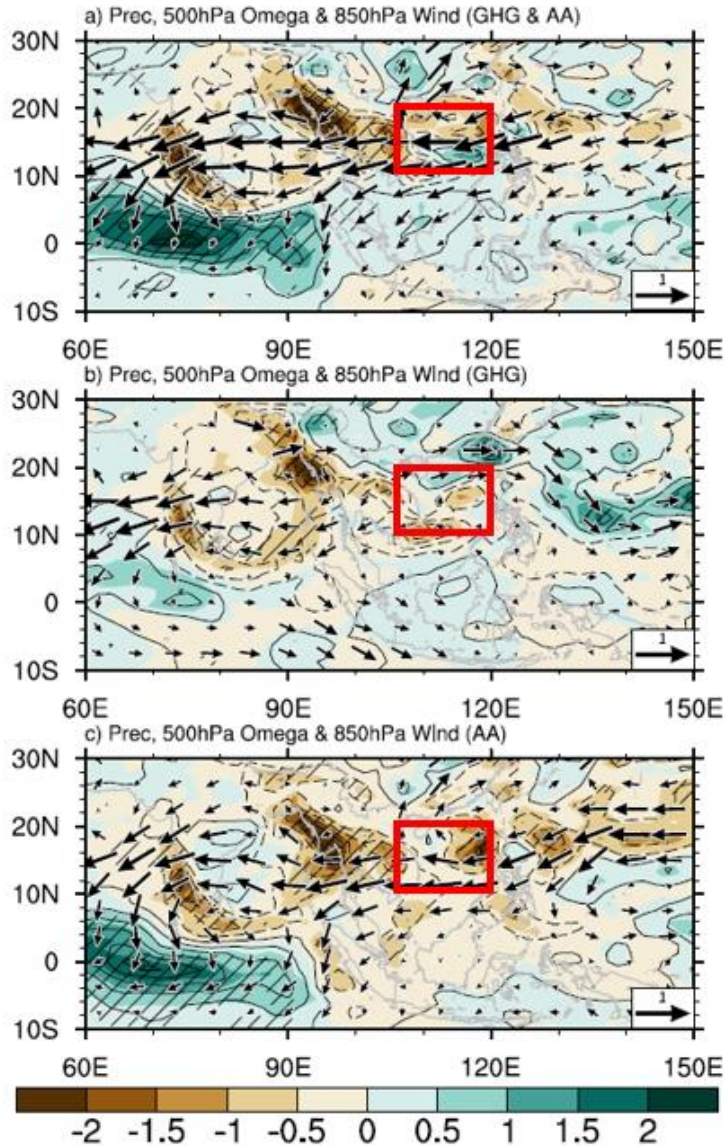
Fig.3 Simulated changes of precipitation (shade, mm/day), 500hPa Omega (contour, 0.01Pa/s) and 850hPa wind (vector, m/s) in JJA. a) Response to anthropogenic forcing (PD-ALL minus EP), b) response to GHG forcing (PD-GHG minus EP), and c) response to AA forcing (PD-AA minus EP) Changes of precipitation in slash regions are statistically significant at the 10% level using a two-tailed Student's t-test. Red box highlights the SCS region.
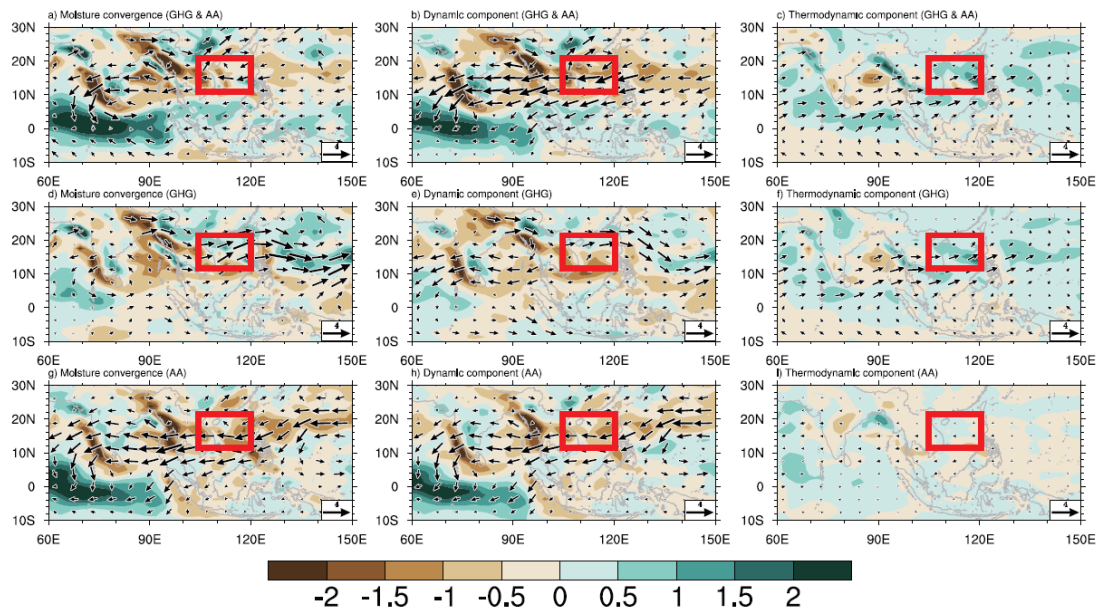
Fig.4. Simulated changes of vertically integrated moisture flux transport (kg/m*s) and its convergence (mm/day) in JJA between PD and EP of All forcing (a, b, c), GHG forcing (d, e, f), and AA forcing (g, h, f). (a, d, g) total moisture flux and its convergence. (b, e, h) dynamic components related to changes in circulation. (c, f, i) thermodynamic components related to changes in humidity. Red box highlights the SCS region.

810
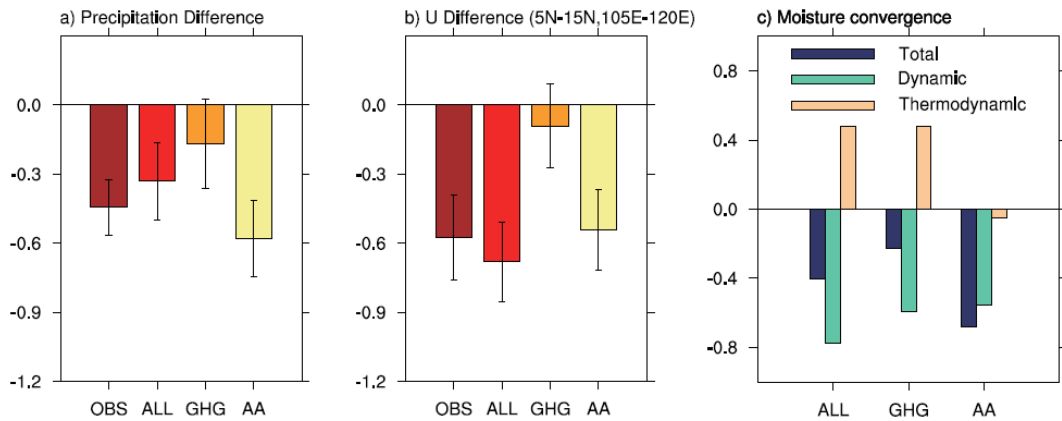
811

812   Fig.5 a) precipitation (mm/day) change between PD and EP in observations

813   (NOAA_PREC), all forcing, GHG forcing and AA forcing over the SCS region (10°N-

814   20°N,105°E-120°E) in JJA.

815   b) zonal wind (m/s) change between PD and EP in observations (NCEP reanalysis 1), all

816   forcing, GHG forcing and AA forcing over south SCS region (5°N-15°N,105°E-120°E) in

817   JJA. The error bars indicate the standard errors of the mean difference。

818   c) simulated change of vertically integrated moisture transport convergence (blue, mm/day)

819   between PD and EP in all forcing, GHG forcing and AA forcing over SCS region (10°N-

820   20°N,105°E-120°E) in JJA. Green bars and yellow bars are the same as blue bars but for

821   dynamic component and thermodynamic component of moisture convergence.

822

823

a) Velocity_potential & divergent wind (850hPa)

b) Velocity_potential & divergent wind (200hPa)

824
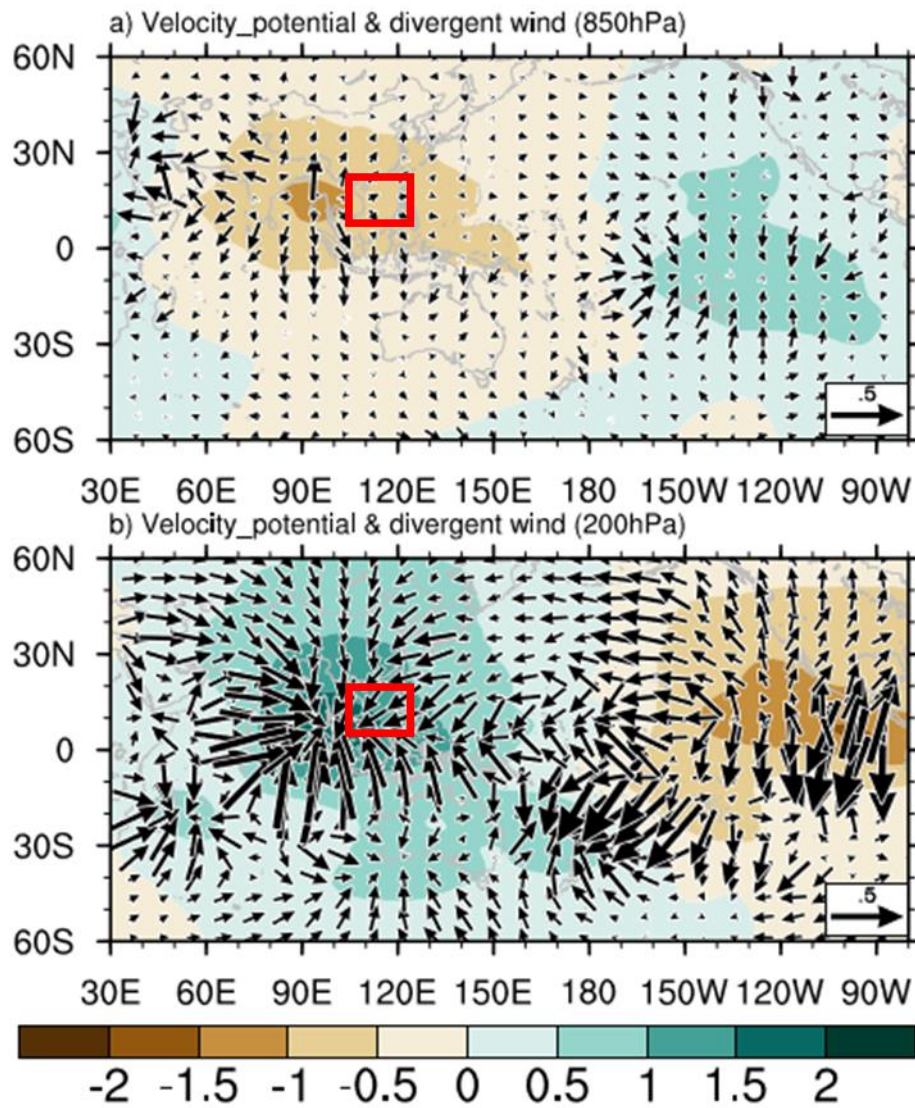
825   Fig.6 Simulated changes in velocity potential (shaded,10^5 m^2/s) and divergent wind

826   (vectors m/s) in JJA in response to GHG forcing (PD-GHG minus EP).   a) at 850hPa,

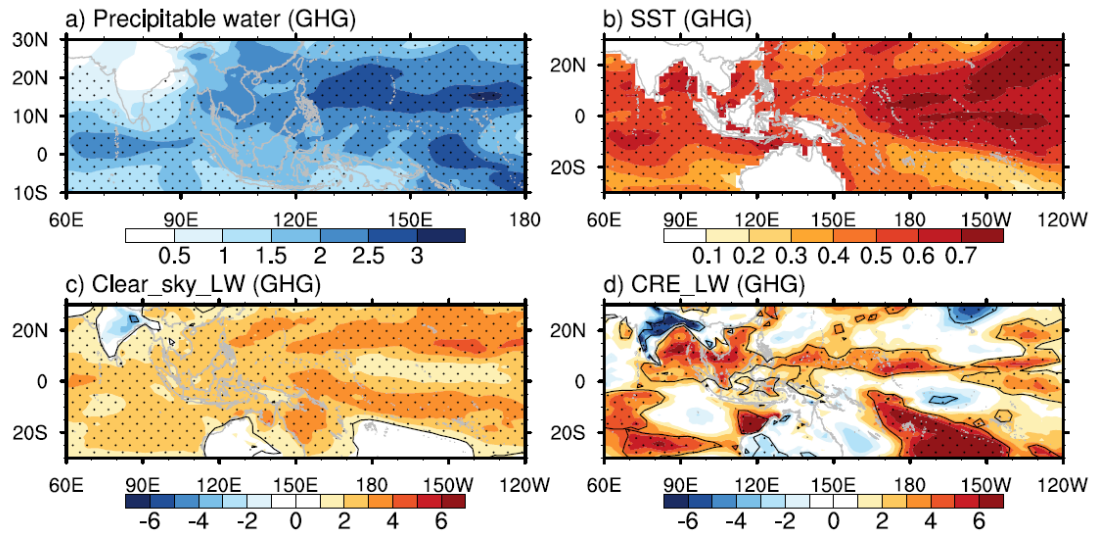827   and b) at 200hPa. Red box highlights the SCS region.

828

829

830

831 Fig.7 Simulated changes in JJA between PD and EP in response to GHG forcing. a)

832 precipitable water (kg/m^2), b) sea surface temperature (℃), c) surface clear sky net

833 longwave radiation (W/m^2), and d) cloud radiative effect of longwave radiation (W/m^2).

834 Radiations are positive downward. Dot regions are statistically significant at the 10% level

835 using a two-tailed Student's t-test.

836

Zonal mean (60° E-150° E) of JJA (AA)

a) meridional circulation

b) SST

837
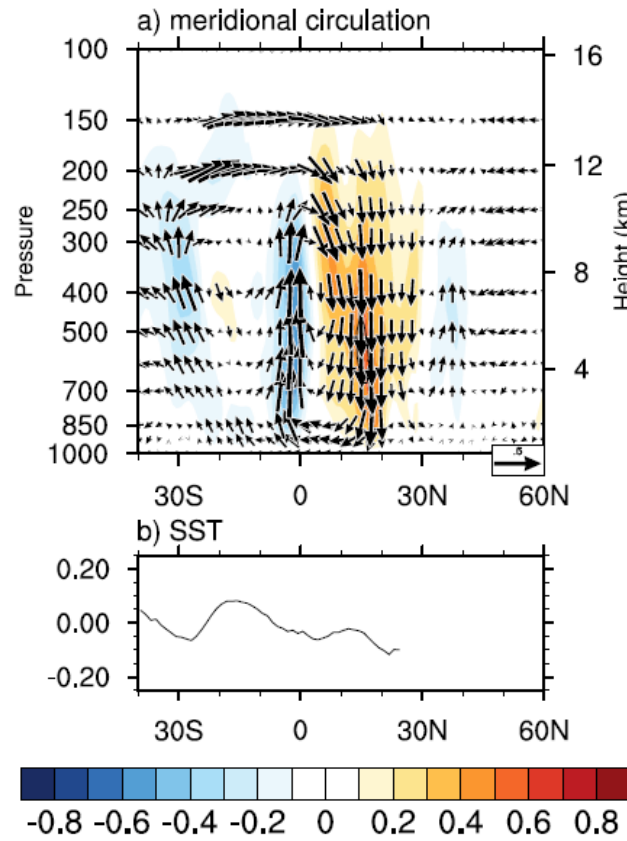
Fig.8 Simulated changes in JJA between PD and EP in response to AA forcing.   a) zonal

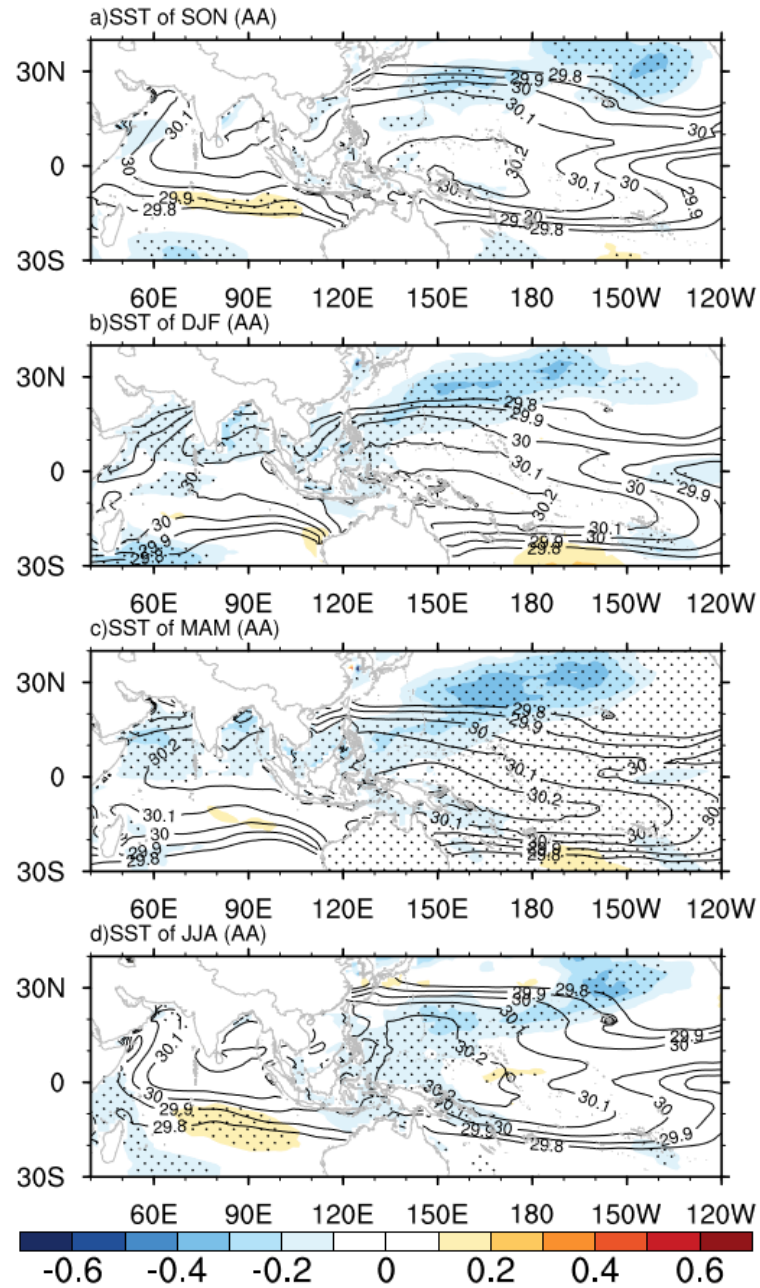mean meridional circulation(vector) and vertical velocity(contour). Unit of meridional wind:

m/s, unit of vertical wind :0.01Pa/s.
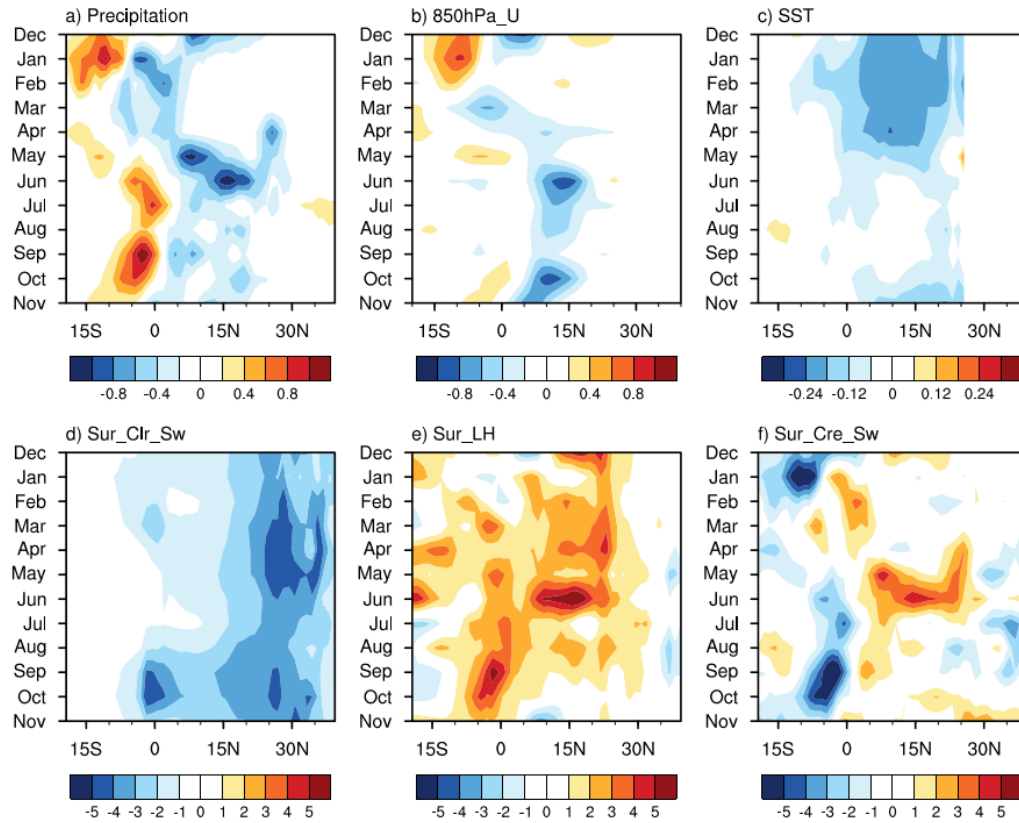
b) zonal mean sea surface temperature (℃).

842

843

844　　Fig.9 Simulated seasonal changes (color, ℃) in sea surface temperature between PD

845　　and EP in response to AA forcing and corresponding climatology (contour, ℃) in the EP

846　　experiment. a) boreal autumn (SON), b) winter (DJF), c) spring (MAM), and d) JJA.　Dot

847　　regions are statistically significant at the 10% level using a two-tailed Student's t-test.

Zoneal mean of 60° E-150° E (AA)

Fig.10 Simulated seasonal evolutions of zonal averaged changes over the sector (60°E-150°E) between PD and EP in response to AA forcing. a) precipitation change (mm/day) b)850hPa zonal wind(m/s), c) sea surface temperature(℃), d) surface clear sky net short wave radiation, e) surface latent heat flux(W/m2), and f) surface cloud radiation effect of short wave radiation (W/m2). Radiation and flux are positive downward.

855

856
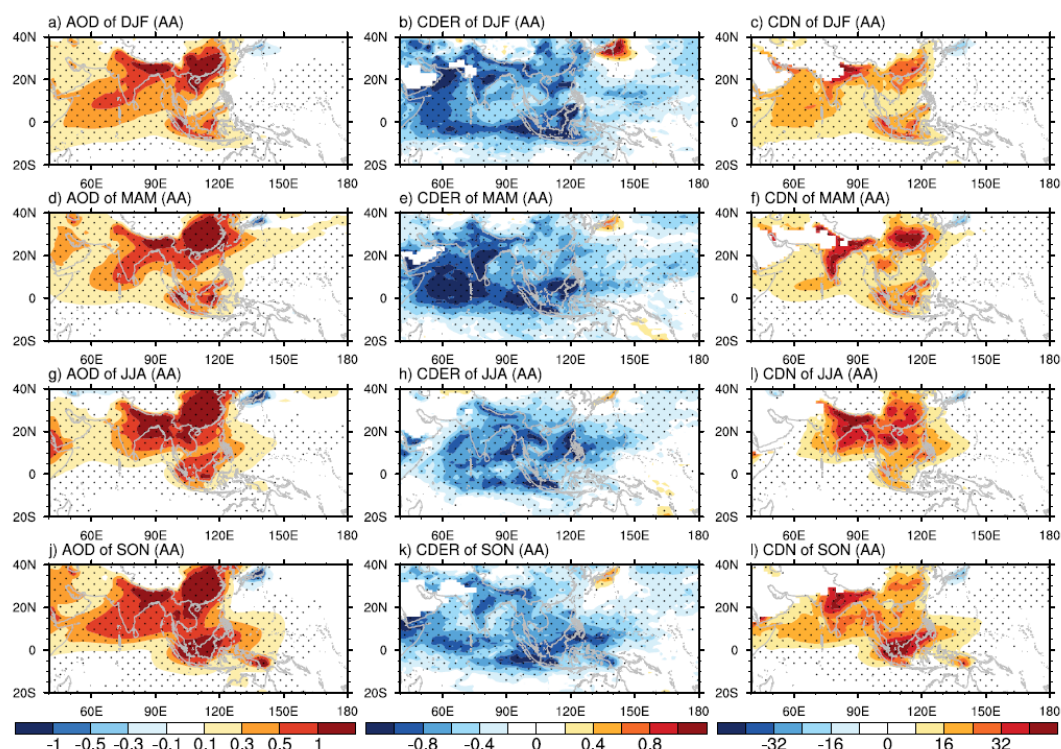
Fig.11 Simulated seasonal changes of aerosol optical depth (AOD, left panels, unit in 0.1)

at 0.55 um, cloud droplet effective radius (CDER, middle panels, unit in um) and cloud

droplet number (CDN, right panels, unit in 10^9 m^{-2}) between PD and EP in response to AA

forcing. a)-c) DJF. d)-f) MAM, g)-h) JJA, j)-l) SON.

861